1987-09

Numerical investigation of orographically enhanced instability

Byrne, Gerald T.

NAVAL POSTGRADUATE SCHOOL
Monterey, California

THESIS

NUMERICAL INVESTIGATION OF OROGRAPHICALLY ENHANCED INSTABILITY

by

Gerald T. Byrne

September 1987

Thesis Advisor: R.T. Williams

Approved for public release, distribution is unlimited

UNCLASSIFIED

ECURITY CLASSIFICATION OF THIS PAGE

REPORT DOCUMENTATION PAGE

a REPORT SECURITY CLASSIFICATION UNCLASSIFIED	1b RESTRICTIVE MARKINGS
a SECURITY CLASSIFICATION AUTHORITY	3 DISTRIBUTION/AVAILABILITY OF REPORT Approved for public release; distribution is unlimited
b DECLASSIFICATION/DOWNGRADING SCHEDULE	
PERFORMING ORGANIZATION REPORT NUMBER(S)	5 MONITORING ORGANIZATION REPORT NUMBER(S)
a NAME OF PERFORMING ORGANIZATION Naval Postgraduate School 6b OFFICE SYMBOL (If applicable) Code 63	7a NAME OF MONITORING ORGANIZATION Naval Postgraduate School
c ADDRESS (City, State, and ZIP Code) Monterey, California 93943-5000	7b ADDRESS (City, State, and ZIP Code) Monterey, California 93943-5000
a NAME OF FUNDING/SPONSORING ORGANIZATION 8b OFFICE SYMBOL (If applicable)	9 PROCUREMENT INSTRUMENT IDENTIFICATION NUMBER
c ADDRESS (City, State, and ZIP Code)	10 SOURCE OF FUNDING NUMBERS PROGRAM ELEMENT NO / PROJECT NO / TASK NO / WORK UNIT ACCESSION NO

1 TITLE (Include Security Classification)

NUMERICAL INVESTIGATION OF OROGRAPHICALLY ENHANCED INSTABILITY

2 PERSONAL AUTHOR(S)

Byrne, Gerald T.

3a TYPE OF REPORT	13b TIME COVERED	14 DATE OF REPORT (Year, Month, Day)	15 PAGE COUNT
aster's Thesis	FROM _____ TO _____	1987, September	60

6 SUPPLEMENTARY NOTATION

7 COSATI CODES			18 SUBJECT TERMS (Continue on reverse if necessary and identify by block number)
FIELD	GROUP	SUB-GROUP	Cyclogenesis; Mountain Effects; Numerical Weather Prediction

9 ABSTRACT (Continue on reverse if necessary and identify by block number)

The NEPRF spectral baroclinic primitive equation model with six layers as numerically integrated over time to examine the effects that vertical ind profiles have on the development of lee cyclogenesis. In addition, he model was run in both linear and nonlinear modes to isolate their ffects on the tests. The objective was to simulate a cold front moving ver a high mountain ridge, similar to the Alps or Rockies, by implementing wind reversal profile and to determine if this was conducive to lee yclogenesis. It was found that the wind reversal profile produced avorable cyclonic growth, particularly when the model was in a linear ode. A nonlinear wind reversal test also produced positive results but nly for a relatively short time; thereafter nonlinear interactions ampened cyclonic growth considerably. In addition, two tests were run

0 DISTRIBUTION/AVAILABILITY OF ABSTRACT	21 ABSTRACT SECURITY CLASSIFICATION
☒ UNCLASSIFIED/UNLIMITED ☐ SAME AS RPT ☐ OTIC USERS	Unclassified
2a NAME OF RESPONSIBLE INDIVIDUAL rof. Roger Williams	22b TELEPHONE (Include Area Code) (408) 646-2296 22c OFFICE SYMBOL Code 63Wu

D FORM 1473, 84 MAR 83 APR edition may be used until exhausted
All other editions are obsolete

SECURITY CLASSIFICATION OF THIS PAGE
UNCLASSIFIED

#19 - ABSTRACT - (CONTINUED)

that allowed the mountain to grow in a very short time to isolate inertial gravity wave interactions. The gravity waves did produce considerable oscillations in the two tests, but after 15 hours or so these two tests showed similar cyclonic growth to the previous tests.

Approved for public release; distribution is unlimited

Numerical Investigation of Orographically Enhanced Instability

by

Gerald T. Byrne
Captain, United States Air Force
B.S., Drexel University, 1974

Submitted in partial fulfillment of the
requirements for the degree of

MASTER OF SCIENCE IN METEOROLOGY

from the

NAVAL POSTGRADUATE SCHOOL
September 1987

ABSTRACT

The NEPRF spectral baroclinic primitive equation with six layers was numerically integrated over time to examine the effects that vertical wind profiles have on the development of lee cyclogenesis. In addition, the model was run in both linear and nonlinear modes to isolate their effects on the tests. The objective was to simulate a cold front moving over a high mountain ridge, similar to the Alps or Rockies, by implementing a wind reversal profile to determine if this was conducive to lee cyclogenesis. It was found that the wind reversal profile produced favorable cyclonic growth, particularly when the model was in a linear mode. A nonlinear wind reversal test also produced positive results but only for a relatively short time; thereafter nonlinear interactions dampened cyclonic growth considerably. In addition, two tests were run that allowed the mountain to grow in a very short time to isolate inertial gravity wave interactions. The gravity waves did produce considerable oscillations in the two tests, but after 15 hours or so these two tests showed similar cyclonic growth to the previous tests.

TABLE OF CONTENTS

LIST OF TABLES

LIST OF FIGURES

I. INTRODUCTION

Considerable interest has been directed to the study of leeside cyclogenesis since Eady's model (1949) described cyclone evolution based on a linear baroclinic mathematical model. Recent models with more realistic topography have simulated mid-latitude cyclones in the lee of large mountain ranges based on specific dynamic mechanisms promoting storm growth.

A recent study by Smith (1986) examined leeside growth with a vertical wind profile similar to a cold front as it passes over a mountain range. Smith's "lee wave theory" utilized a 3-dimensional linear quasi-geostrophic model which predicted with partial success the time scale, position, size and strength of a leeside low. Based on this theory, Smith discovered that a leeside low would grow dramatically if a lid, which represents a tropopause and thus would allow for baroclinic instability, was introduced. He found that this low would grow at first by orographic forcing, then would grow exponentially by the baroclinic instability mentioned above. Thus, there were two stages of cyclone development. However, the initial rapid growth was not evident when the wind profile did not reverse with height. When Smith compared his theoretical results with actual Alpine lee cyclogenesis cases, he found good

qualitative but poor quantitative agreement. Some suggestions he proposed to improve on his work were the inclusion of factors such as nonlinearity, mesoscale and low-level blocking, and more accurate modeling of the width of an approaching baroclinic zone.

Hayes (1985) investigated three dynamic mechanisms which previous studies indicated might be influential in mid-latitude leeside cyclogenesis. The three mechanisms were enhanced leeside baroclinic instability, continuous-mode growth and superposition. Two atmospheric models were used to study these mechanisms. The UCLA finite-difference model and a spectral model, developed by NEPRF by Dr. T. Rosmond, were implemented to study these dynamic mechanisms. The terrain resembled the Rocky Mountains and Hayes varies the width of a jet with positive shear (i.e, winds not reversing with height), to simulate normal tropospheric flow over the Rockies. A wide jet which approximated a realistic baroclinic zone flowing over a high and long mountain ridge, with the superposition mechanism involved, gave the most impressive results. He concluded that the orographic forcing mechanism may be the catalyst needed when a baroclinic zone coincides with this natural leeside trough. It also appeared that a higher mountain ridge forced a deeper leeside trough to promote cyclogenesis.

The objective of this paper is to determine if a vertical wind profile with a height reversal is a key factor

in leeside cyclogenesis. The work of Smith and Hayes formed the basis of this study. Chapter II describes the atmospheric model used in this study. It is one of the models used by Hayes in his work. It is the NEPRF nonlinear primitive equation spectral model (Rosmond) and is used in this research since it can be run in both a linear and nonlinear form. In Chapter III, the vertical wind profiles, the initial baroclinic disturbance and the topography are mathematically detailed. Chapter IV gives the results of the two control tests (flat terrain) and six mountain experiments. Two vertical wind profiles, one reversing and the other not reversing in height are each tested in both linear and nonlinear modes. The last two tests are run in a linear mode, but the mountain growth time was only three hours as compared to the 36-hour growth period for the first four mountain tests. Thus a comparison can be made for each respective wind profile based on linearity and initialization time that might indicate peculiarities of the atmospheric model itself. The main variable analyzed is the maximum deviation from the longitudinal averaged vorticity (ξ'_{max}) and its phase, so a comparison of growth rates and its position and movement can be made between all tests. While ξ'_{max} does not give a truly accurate growth factor, it is sufficient to determine if leeside development may occur.

II. MODEL DESCRIPTION

The model used in this study is a baroclinic spectral transform model developed by Dr. T. Rosmond for NEPRF. A detailed description of this model is given by Lubeck, Rosmond and Williams (1977). A short summary of this model, implemented here, follows.

The spectral model encompasses the nonlinear primitive equations for an adiabatic and hydrostatic atmosphere. Friction is also included, but moisture (i.e., latent heat) and its effects are not. The basic equations in sigma coordinates are as follows:

$$\frac{\partial \xi}{\partial t} = -\vec{\nabla}\cdot(\zeta+f)\vec{V} - \vec{k}\cdot\vec{\nabla}\times(RT\vec{\nabla}q + \dot{\sigma}\frac{\partial \vec{V}}{\partial \sigma}) + \vec{k}\cdot\vec{\nabla}\times\vec{F} \qquad (2.1)$$

$$\frac{\partial D}{\partial t} = \vec{k}\cdot\vec{\nabla}\times(\zeta+f)\vec{V} - \vec{\nabla}\cdot(RT\vec{\nabla}q + \dot{\sigma}\frac{\partial \vec{V}}{\partial \sigma}) - \vec{\nabla}^2(\phi+\frac{\vec{V}^2}{2}) + \vec{\nabla}\cdot\vec{F} \qquad (2.2)$$

$$\frac{\partial q}{\partial t} = -D - \vec{V}\cdot\vec{\nabla}q - \frac{\partial \dot{\sigma}}{\partial \sigma} \qquad (2.3)$$

$$\frac{\partial \theta}{\partial t} = -\vec{V}\cdot\vec{\nabla}\theta + \dot{\sigma}\frac{\partial \theta}{\partial \sigma} + \frac{Q}{PCp} \qquad (2.4)$$

$$\frac{\partial \phi}{\partial \sigma} = -\frac{RT}{\sigma} \qquad (2.5)$$

where:

ζ = vorticity

D = divergence

T = temperature

θ = potential temperature

π = surface pressure

V = horizontal velocity vector

ϕ = geopotential height

R = gas constant

Cp = specific heat at constant pressure

f = Coriolis parameter

σ = vertical coordinate ($\sigma = p/\pi$)

$\dot{\sigma}$ = vertical velocity ($\dot{\sigma} = \frac{d\sigma}{dt}$)

q = $\ln \pi$

p = p^k

k = R/Cp

F = frictional force

λ = longitude

ϕ = latitude

X = $\sin \phi$

The model's prognostic variables are the vorticity and divergence of the wind (q,D), temperature (T), and the natural log of terrain pressure ($q = \ln p_s$). The vertical coordinate is defined as

$$\sigma = \frac{P - P_t}{P_s - P_t},$$

where p_s is the surface pressure and p_t is the top of the model atmosphere. In this study p_t = 0 mb.

Equations 2.1 through 2.5 are transformed into spherical coordinates and are represented spectrally in the horizontal, while finite differences are used in the vertical.

The vertical structure of the model follows the development given by Arakawa and Suarez (1983). In this study only six layers which are equally spaced in sigma are used (Figure 2.1). The prognostic variables listed above are represented spectrally in the horizontal and are staggered in sigma so that ξ, D, U, V, and T are carried at the mid-point of each layer and $\dot{\sigma}$ is carried at the top and bottom of each layer. The vertical vorticity, $\dot{\sigma}$, is assumed to vanish at the upper and lower boundaries.

Two versions of the model are used in this study. The linear version utilizes one wavelength in the east-west direction, while the nonlinear version employs three wavelengths. The wavenumbers when used in nonlinear spectral formulation are 8 for the linear version, and 0, 8 and 16 for the nonlinear mode. Each version is accomplished by forcing the time tendencies to be zero at all wavenumbers except for the wavenumbers employed. Cyclic continuity is assumed in the model.

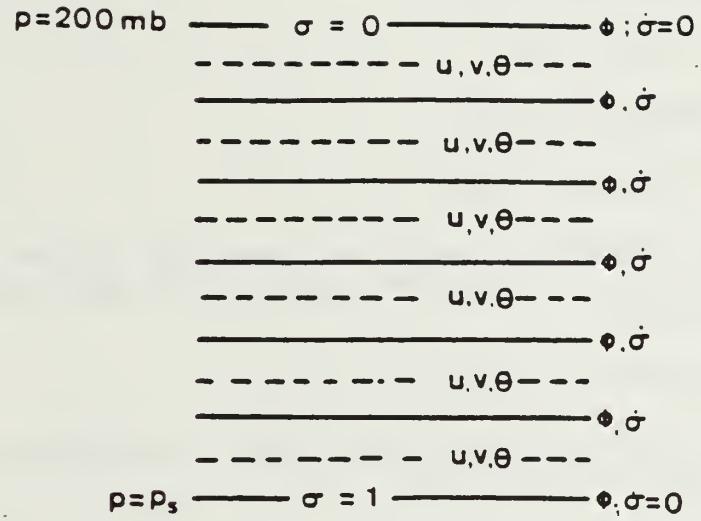

Figure 2.1 Vertical Structure of the Spectral Model

The spectral formulation of the variables in the horizontal are represented by the following equation:

$$C(\lambda, x, \sigma, t) = \sum_{m=-J}^{J} \sum_{n=|m|}^{J} C_n^m(\sigma,t) P_n^m(x) e^{im\lambda}$$

$$= \sum_{m=-J}^{J} \sum_{n=|m|}^{J} C_n^m Y_n^m \qquad (2.7)$$

where:

C = some variable

$(C_n^m)^* = (-1)^m C_n^{-m}$

m = zonal wavenumber

n = meridional index

$n-|m|$ = the number of zeros between the poles ($-1 \leq x \leq 1$) of the associated Legendre function

J = truncation limit

λ = (l-1)/2 nondimensional zonal coordinate index ($1 \leq l \leq 16$)

The nonlinear terms are computed using the transform method described by Haltiner and Williams (1980). The longitudinal direction is treated with a Fast Fourier Transform and the latitudinal direction uses Gaussian Quadrature. The number of latitudes, N, and longitudes, M, satisfy

$$N \geq \frac{2}{3}J + 1, \qquad M \geq 3J + 1$$

The number of points are chosen so there will be aliasing from the product terms. For this study N = 38, and M = 16.

III. INITIAL CONDITIONS

The initial wind profile and terrain are the same as described by Hayes (1985). A brief description of these initial parameters will be discussed below.

Hayes stated that the initial jet structure should be carefully selected since the vertical and horizontal structure of the mean tropospheric flow plays a significant role in the development of a cyclone. In addition, the size, scale and orientation of a mountain ridge can affect the frequency of cyclogenesis. Although the topography adopted from Hayes' study resembles the Rocky Mountains, it appears sufficient for this study since we are primarily concerned with a wind structure that would best promote cyclogenetic growth in the lee of the Alps. Those conditions include a cold front (i.e., winds reversing with height) traversing the Alpine region.

A. MEAN WIND STRUCTURE

The complete wind profile is expressed as:

$$\bar{u}[\phi, p(\sigma,\phi)] = -\Omega a \cos\phi + \Omega a \cos\phi \left[1+2(\bar{u}_u+\bar{u}_s)/\Omega a \cos\phi\right]^{0.5} , \qquad (3.1)$$

where a is the radius of the earth, Ω is the earth's rotation rate. $\bar{u}_u$ is the upper level wind current and can be expressed as:

$$\bar{u}_u[\phi, p(\sigma,\phi)] = \bar{\bar{u}}_o \, \mathrm{sech}^2[\gamma(\phi-\phi_o)](\ln(p_s/p)/\ln(p_s/p_{max}) , \tag{3.2}$$

where $\bar{\bar{u}}_o$ = 65 m/s, ϕ_o = 45 N, p_s = 1013.25 mb, p_{max} = 200 mb and γ is the halfwidth of the jet. In this study γ = 16, which excludes barotropic instability. $\bar{u}_s$, the mean surface current, is expressed as:

$$\bar{u}_s(\phi) = \bar{u}_{oo}\mathrm{sech}^2[\gamma(\phi-\phi_o)] \tag{3.3}$$

where $\bar{u}_{oo}$ = -20 m/s or +20 m/s depending on whether a wind reversal or a non wind reversal is implemented. The v component for the mean wind structure is set to zero at all levels. Figures 3.1 and 3.2 show the mean wind structure for the wind reversal and non-reversal profiles respectively in three dimensions. Thus we see that the wind speed varies linearly with the log of pressure while its latitudinal variation is that of a Bickley jet as described by Haltiner and Williams.

B. DISTURBANCE

The initial disturbance used in this study, which is adopted from Hayes (1985), is a barotropic disturbance that will permit us to study the effect of topography on a

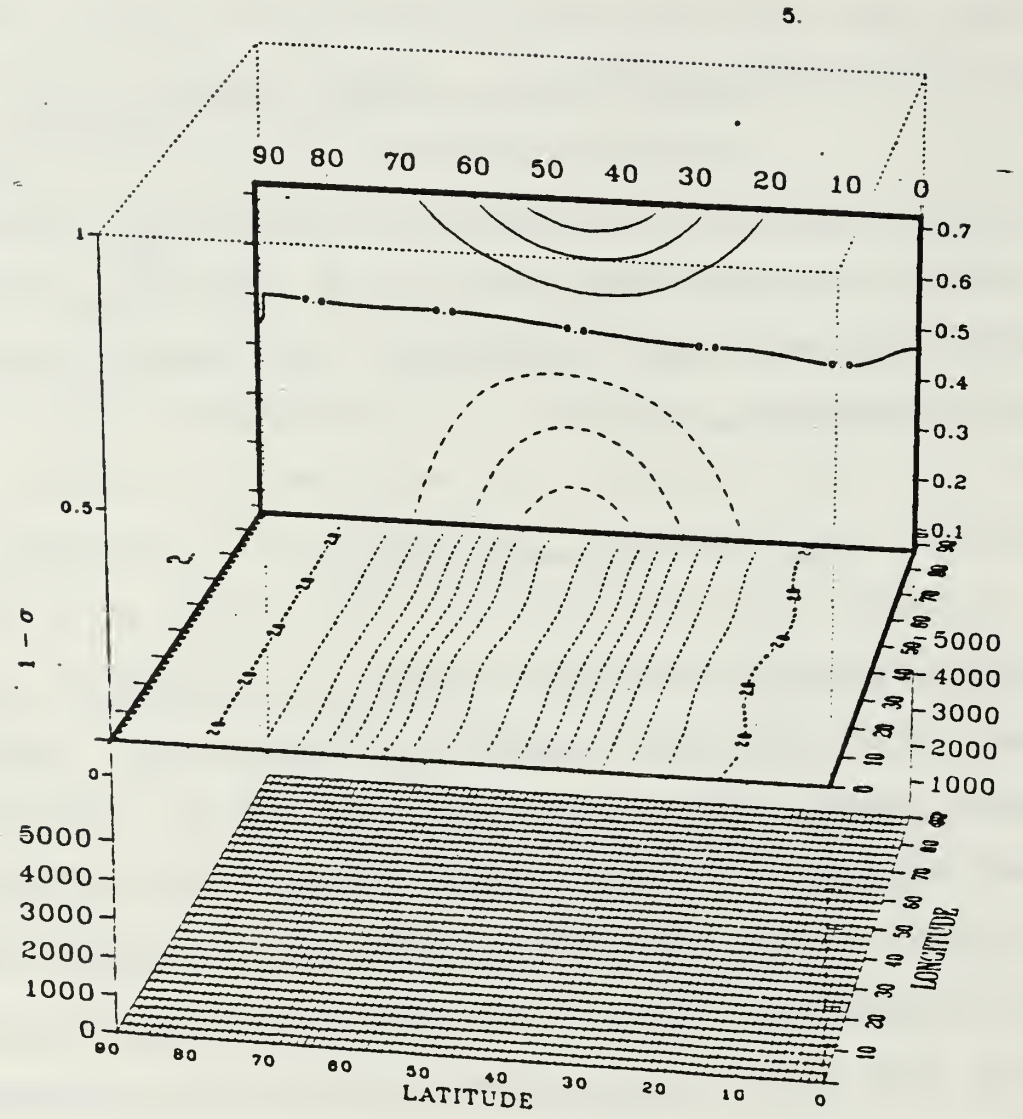

Figure 3.1 3-dimensional Structure of the Mean Wind Profile for the Wind-reversal Tests at t = 0

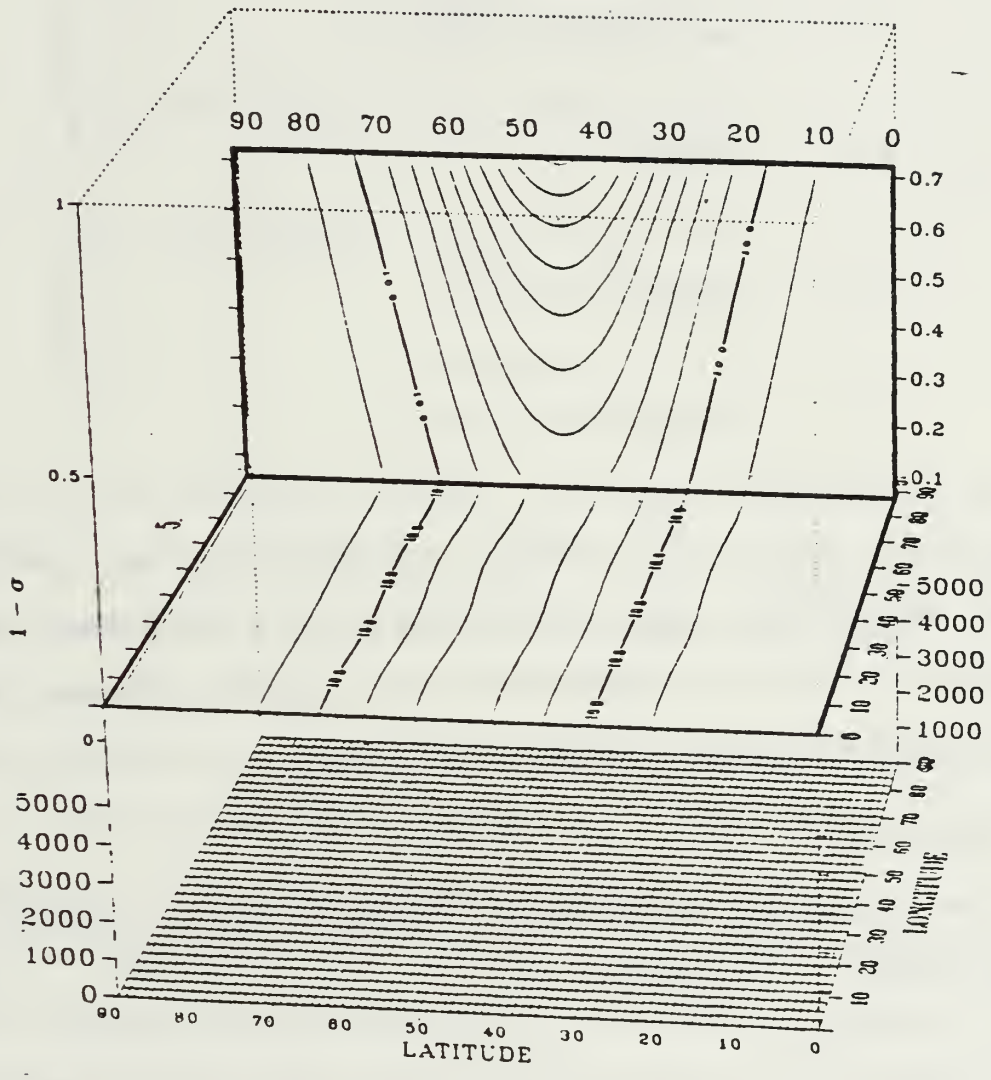

Figure 3.2 Same as Figure 3.1, Except for Non Wind-reversal Tests

baroclinic wave. It consists of a weak wave which varies sinusoidally with longitude and has a maximum amplitude at 45° N. The geostrophically balanced fields are expressed as:

$$\begin{aligned} \Phi' &= f_o[A^* \sin(n\lambda)\sin^2(2\phi)] \\ p' &= \bar{p}\Phi'/R\bar{T} \\ u' &= -(1/f_o a)\ \partial\Phi'/\partial\phi \\ v' &= 1/(f_o a \cos\phi)\ \partial\Phi'/\partial\lambda\ , \quad T' = 0 \end{aligned} \tag{3.4}$$

where $\bar{T}$ = 273 K, $\bar{p}$ = 1013.25 mb and λ is the longitude. Hayes determined that wavenumber = 8 exhibited maximum growth and is the wavenumber used in this study for the linear version of the model.

C. TERRAIN

The topography implemented in this study is adopted from Hayes (1985). It is given by

$$z_m(\phi,\lambda) = \begin{cases} z_*(\phi)\cos^2\left[\left(\frac{\lambda-\lambda_o}{4\Delta\lambda}\right)\frac{\pi}{2}\right] , & |\lambda-\lambda_o| \leq 4\Delta\lambda \\ 0 , & |\lambda-\lambda_o| \geq 4\Delta\lambda , \end{cases} \tag{3.5}$$

where $\Delta\lambda$ is the longitudinal grid spacing and λ_o is the longitude where the mountain is centered. In this study $\lambda_o = 22.5^o$. $Z^*(\phi)$ is expressed by

$$z_*(\phi) = \begin{cases} z_s & , \ \phi_N > \phi > \phi_S \\ z_s \cos^2\left[\left(\frac{\phi-\phi_N}{3\Delta\phi}\right)\frac{\pi}{2}\right] & , \ \phi_N + 3\Delta\phi \geq \phi > \phi_N \\ z_s \cos^2\left[\left(\frac{\phi-\phi_S}{3\Delta\phi}\right)\frac{\pi}{2}\right] & , \ \phi_S > \phi \geq \phi_S - 3\Delta\phi \\ 0 & , \ \text{elsewhere} , \end{cases} \tag{3.6}$$

where z_s is the mountain weight, $\Delta\phi$ is the latitudinal grid spacing, ϕ_N is approximately 61.75 N and ϕ_S is 31.25 N. Thus, the mountain is 22.5^o wide and extends from about 73^oN to 20^oN (see Figure 3.2).

The mountain is allowed to grow to its full height at time t_o. For this study's purposes t_o = 36 h for most test runs and t_o = 3 h for two special tests.

Inertial gravity wave growth is reduced effectively using the longer growth time while the shorter growth time permits us to see their influence. The time increment scheme used to allow the mountain to reach its full height is:

$$z_m(\lambda, \phi, t) = \begin{cases} z_{m*}(\lambda,\phi) \sin^2\left(\frac{\pi t}{24}\right) \\ z_{m*}(\lambda,\phi) \end{cases} \tag{3.7}$$

Walker (1982) and others have found that smooth and rapid adjustments occur with this method.

It is found in this study that the desired mountain height of 3000 m is truncated by the spectral parameters mentioned in Chapter II. Thus, the resulting height of the mountain in this study is 2213 m. However, it is felt this height is sufficient for our purposes since we are primarily concerned with wind profiles most conducive to cyclogenesis.

IV. RESULTS

A. CONTROL RUNS

Control runs with terrain heights set to zero over the entire sector are made for both the wind reversal and non-reversal profiles. The initial disturbance described in Section III.B is used in both control runs as well as the mountain experiments in the next section. The wind profile parameters for the jet structure of the control experiments are:

Case A: $u_s = -20$ m/s, $u_u = 65$ m/s

Case B: $u_s = 20$ m/s, $u_u = 65$ m/s

The primitive equation spectral model utilizes wavenumber 8 in its linear form since this wavenumber is most conducive for instability and growth (Hayes, 1985).

Two atmospheric levels are used in all test cases to determine the vertical difference in vorticity growth and phase speed. The levels are designated as L = 3 and L = 6, where $L = 1/2 + \sigma/b\sigma$ and they roughly correspond to a mid-tropospheric height and a boundary layer top respectively.

The maximum of the deviation from the longitudinal averaged vorticity, ξ'_{max}, and its phases are analyzed for

comparison with the mountain experiments in the next section. The perturbed vorticity component is observed to measure cyclone development while the phase is used to determine movement of the developing cyclonic vortex. These are used for comparison against the mountain experiments.

Figures 4.1 and 4.2 show the perturbed vorticity component, ξ'_{max}, versus time and Table 4.1 lists the average growth of ξ'_{max} from t_o to $t_o + 36$. The perturbed vorticity element for case B grows at a slightly larger rate than case A at the upper level (L = 3). At the lower level the growth rates are nearly identical. The upper level growth is greater in the non wind-reversal case due to a larger mean flow at that level (i.e., more of a shear component of vorticity). It appears that the wind reversal case has no advantage over the non wind-reversal case when there is no topography.

The analysis of the phase speeds (Table 4.2) at ξ'_{max} reveals that case A retrogrades at the rate of -6.4 deg/day at L = 3 and -6.1 deg/day at L = 6. Case B results for the same respective levels are 27.0 and 26.2 deg/day. This would appear to be reasonable since the mean wind speed of the non-reversal case is considerably larger. This may also suggest that the possibility for cyclone development on the lee of mountains may require a mean phase speed close to stationarity and the wind reversal profile would fit that prerequisite.

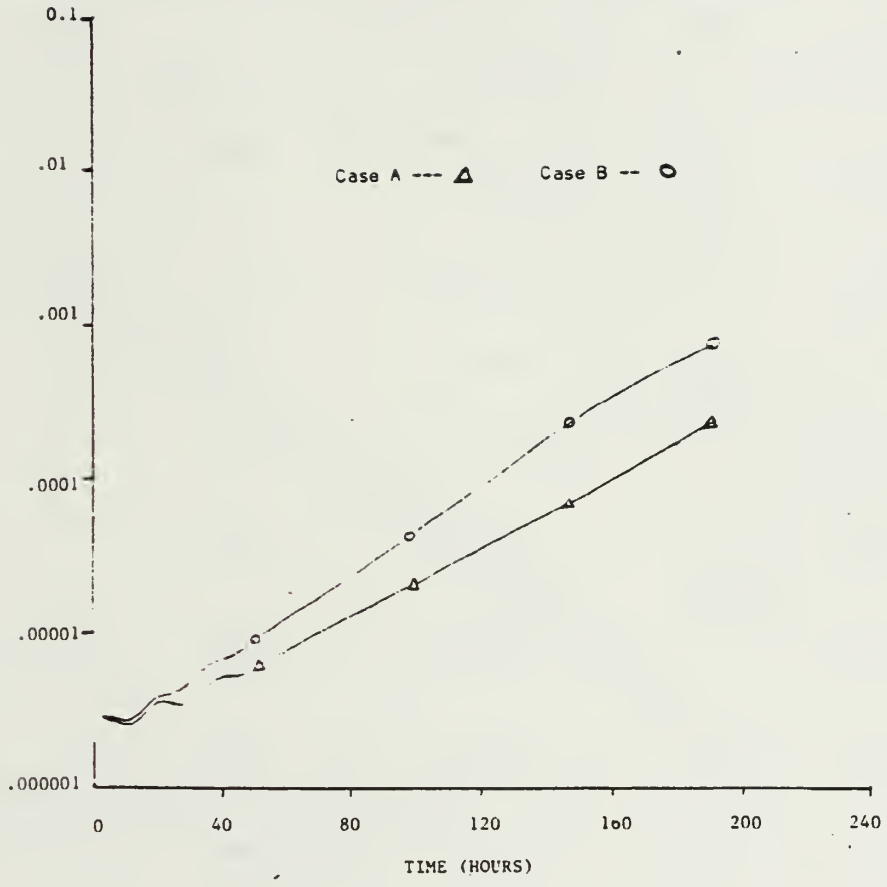

Figure 4.1 Maximum Deviation from the Longitudinally Averaged Vorticity, ξ'_{max} vs. Time at Tropospheric Level, L = 3, for Cases A and B

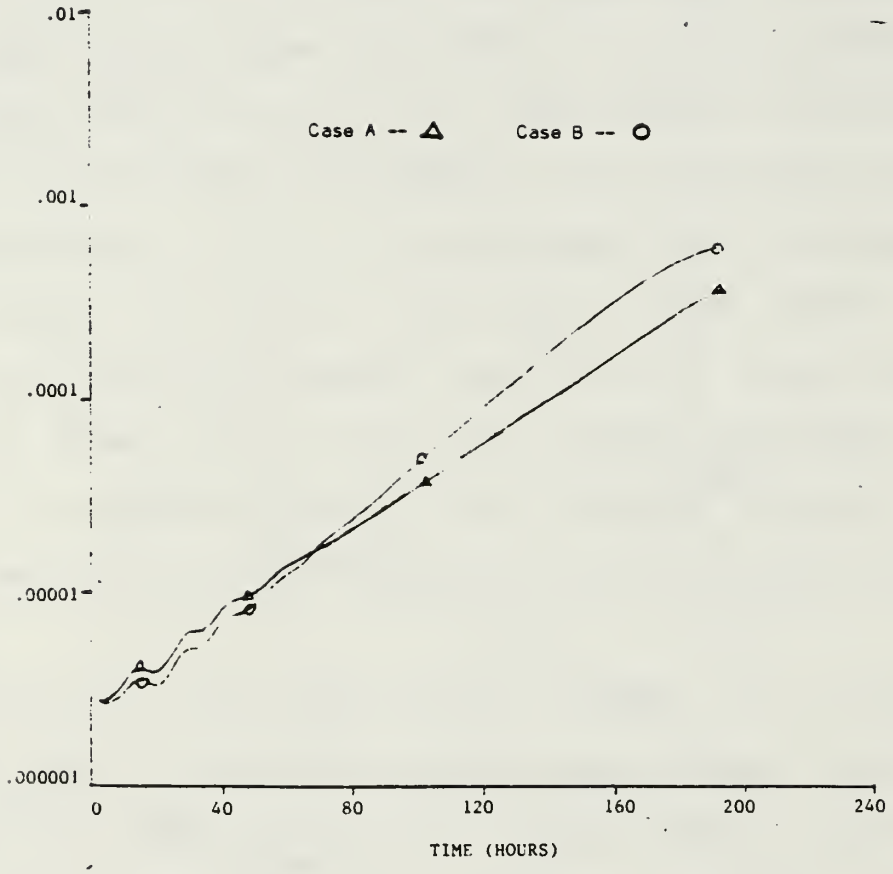

Figure 4.2 Same as Figure 4.1, Except L = 6 for Cases A and B

TABLE 4.1

AVERAGE GROWTH OF ξ'_{max} FOR ALL TEST RUNS

	L = 3	L = 6	L = 6/L = 3
Case A	.16	.32	2.00
Case B	.35	.37	1.06
Test 1	2.51	5.31	2.16
Test 2	.40	.37	.93
Test 3	.42	.94	2.23
Test 4	.48	-1.69	-3.52
Test 5	1.80	4.31	2.39
Test 6	.88	.06	.07

TABLE 4.2

AVERAGE PHASE SPEED OF ξ'_{max} FOR ALL TEST RUNS

	L = 3	L = 6
Case A	-6.34	-6.10
Case B	27.01	26.24
Test 1	-4.86	-6.72
Test 2	28.08	27.84
Test 3	12.01	-10.50
Test 4	25.96	24.11
Test 5	-6.40	-0.83
Test 6	26.27	28.12

Thus, overall inspection does not permit one to determine which wind profile is most conducive for cyclogenesis when no mountain is imposed on the mean atmospheric flow.

B. MOUNTAIN TESTS

The initial field conditions for the mountain experiments are the same as for the control runs described in Section IV.A. As mentioned previously in Chapter III, the mountain depicted is grossly similar in shape to the Rocky Mountains, but should be sufficient to use since the wind reversal phenomenon that is encountered in the Alpine Leeside situation is the main focus of this study. The mountain is allowed to grow to its full height (2213 m) by the 36th hour for the first four test runs to minimize the impact of the inertial gravity waves generated by the model. The height of the mountain was originally intended to be 3000 m but a truncation error in the spectral representation produced the 2213 m height. However, it appears this height does not seriously degrade the output, so additional runs are not required. The last two test runs permit the mountain to grow to its full height in just three hours to isolate the gravity wave phenomenon. The test runs and their critical parameters are:

Test 1, Linear, Wave # = 8, Wind reversal (u_s = -20 m/s, u_u = 65 m/s), Mountain growth period (MGP) = 36 h.

Test 2, Linear, Wave # = 8, Non-reversal (u_s = 20 m/s, u_u = 65 m/s), MGP = 36 h.

Test 3, Nonlinear, Wave # = 0, 8, 16, Wind reversal, MGP = 36 h.

Test 4, Nonlinear, Wave # = 0, 8, 16, Non wind-reversal, MGP = 36 h.

Test 5, Linear, Wave # = 8, Wind reversal, MGP = 3 h.

Test 6, Linear, Wave # = 8, Non wind-reversal, MGP = 3 h.

As in the control runs, the maximum deviation from the longitudinally averaged vorticity, ξ'_{max}, and its phase position and speed are examined.

1. Linear Tests

Utilizing the linear version of the primitive equation spectral model, tests 1, 2, 5 and 6 are run with the same wavenumber (8) as the control runs. The nonlinear versions, tests 3 and 4, utilized wavenumbers 0, 8 and 16. Thus the behavior of the spectral model can be explored in both the linear and nonlinear modes.

Before examining the results one can assume that the nonlinear solutions would limit the exponential growth inherent in a linear solution and the nonlinear mode would more closely approximate a real-world scenario. In addition, the linearized tests would serve as a benchmark to other studies employing linear theory (e.g., Smith, 1984, 1986).

Figures 4.3 and 4.4 contain the maximum deviation from the longitudinal averaged vorticity, ξ'_{max}, versus time for the linear mountain experiments as well as the results from the two control runs. At the upper level, L = 3, Test

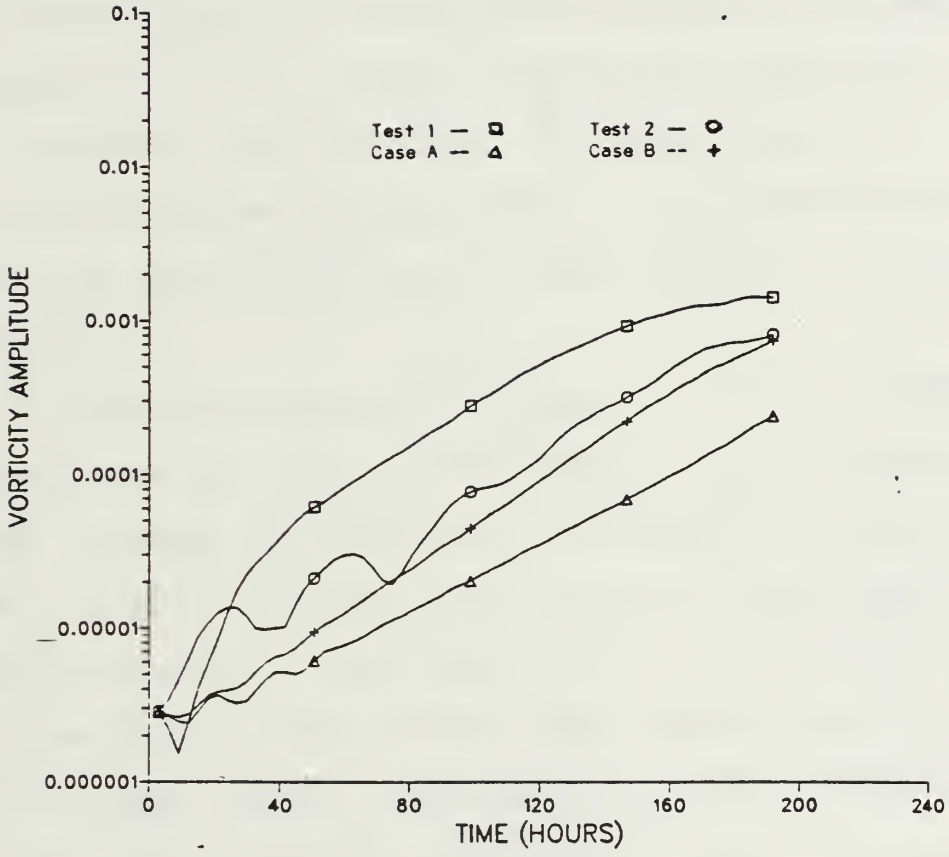

Figure 4.3 Same as Figure 4.1, Except L = 6 for Cases A and B

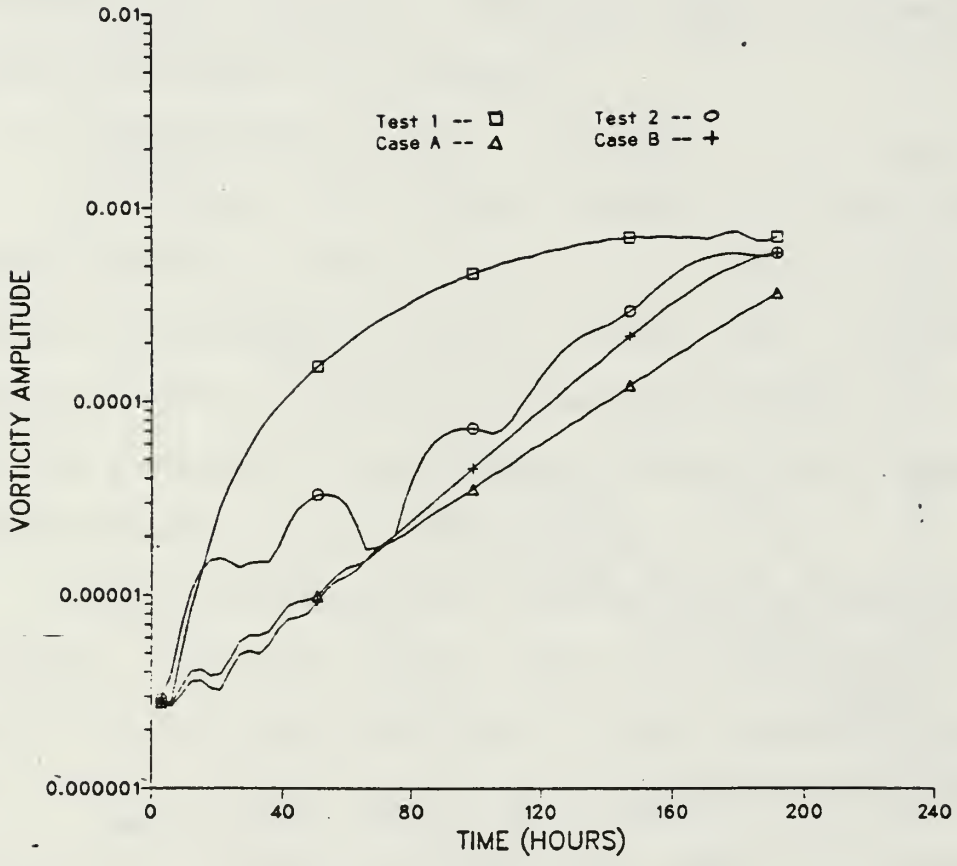

Figure 4.4 Same as Figure 4.1, Except for Cases A and B and Tests 1 and 2 at L = 6

1 exhibits the largest growth from t_o to t_o + 36. Its average growth during this period is over six times larger than test 2 (see Table 4.1). At the lower level test 1 experienced a growth rate 14 times larger than test 2. Comparing test 1 to the control runs, where the topography was set to zero, the comparison was even larger whereas the non-reversal cases exhibited no significant change at either tropospheric level. Thus the mountain experiment with a wind reversal profile, test 1, experiences the largest cyclonic development particularly at the top of the boundary layer and during the period when leeside development is favorable.

The phase position of ξ'_{max} in tests 1 and 2 and the control runs are shown in Figures 4.5, 4.6, 4.7 and 4.8. A smooth average was performed to derive a reliable phase speed. Table 4.2 lists these results. Important findings from this table are that test 1 has a retrograding speed at both atmospheric levels while test 2 has a steady and large positive phase speed. Composite results indicate that all of the wind reversal experiments have a retrograding perturbed vorticity maximum.

Table 4.3 lists the position of ξ'_{max} at both levels for all tests and control runs from t_o through t_o + 36. ξ'_{max} at L = 3 in test 1 is slightly behind (upstream or to the west of) the maximum at L = 6. Test 2, the non-reversal case, also has the lower level maximum ahead (west) of the

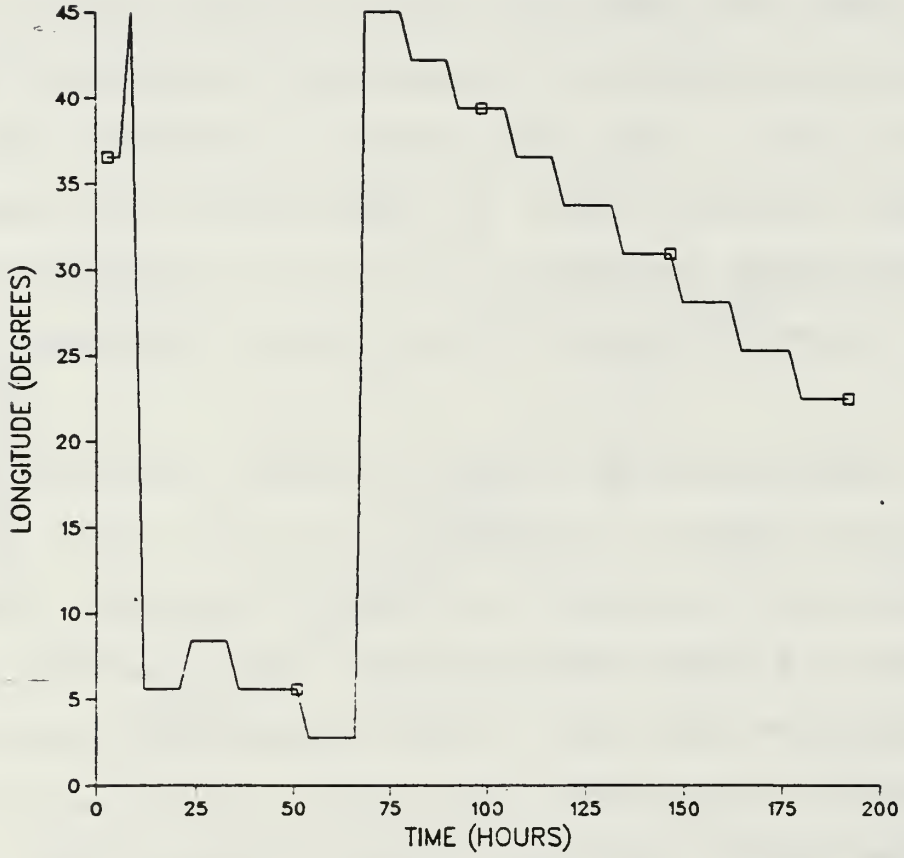

Figure 4.5 Test 1; Phase Position of ξ'_{max} vs. Time at L = 3

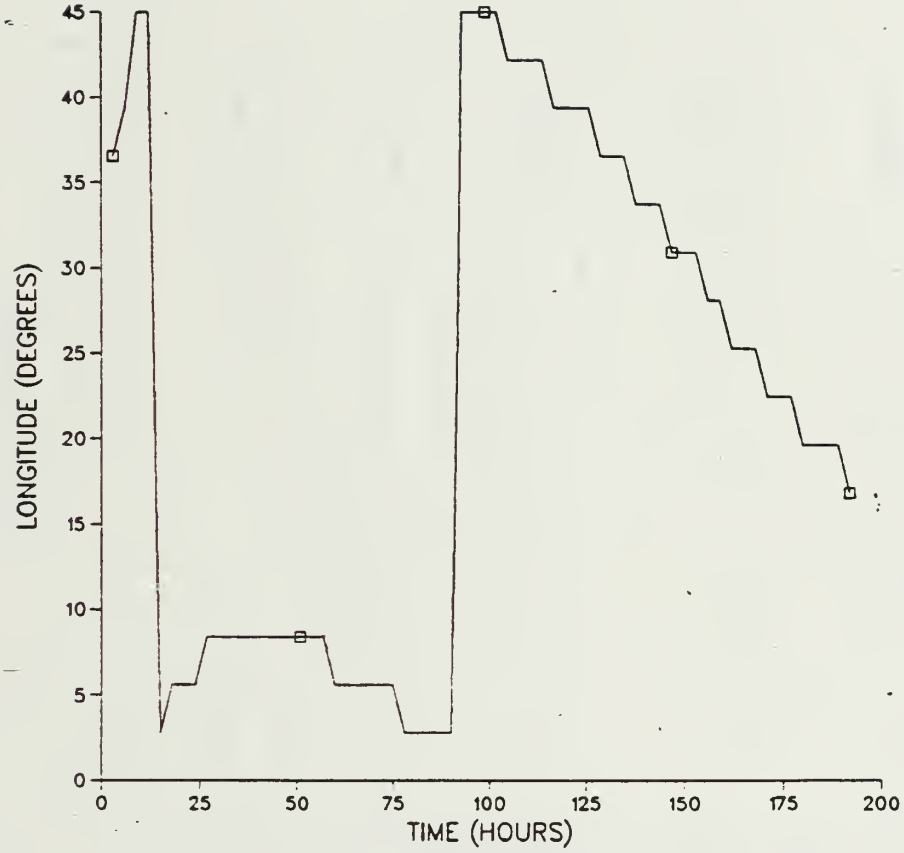

Figure 4.6 Same as Figure 4.1, Except for Test 1 and L = 6

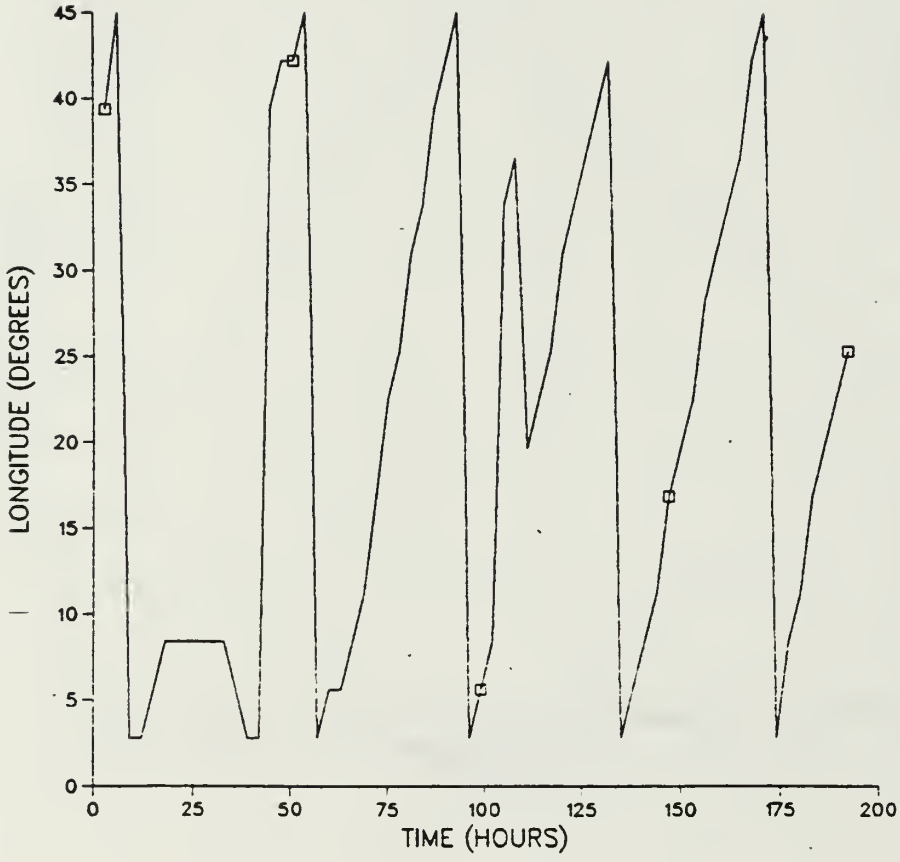

Figure 4.7 Same as Figure 4.1, Except for Test 2 and L = 3

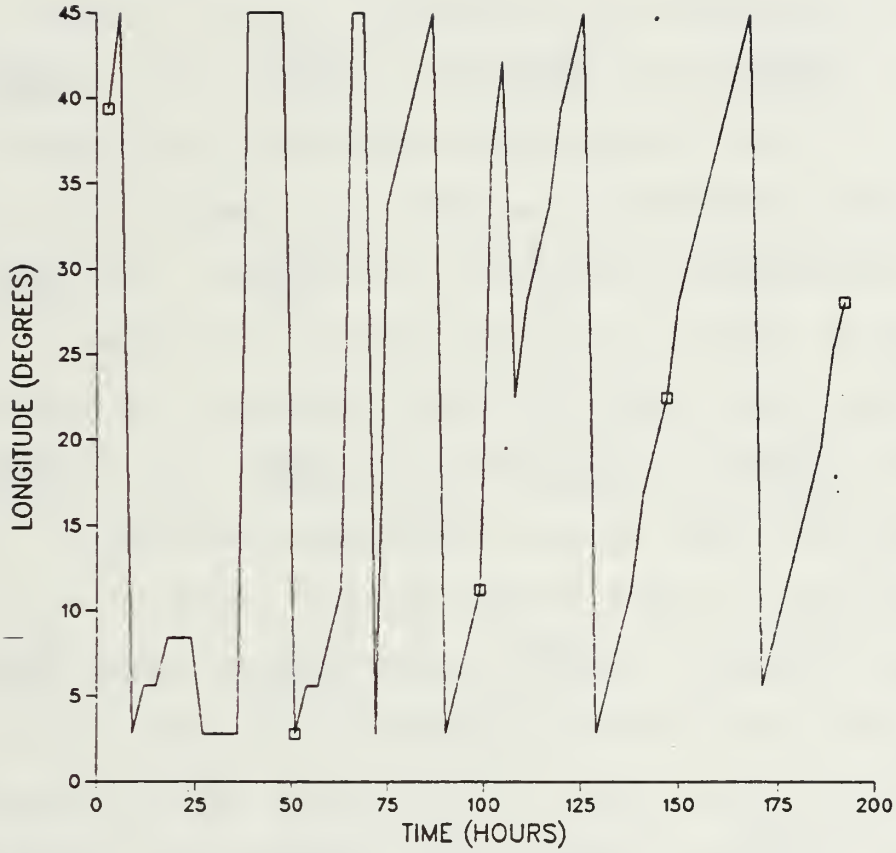

Figure 4.8 Same as Figure 4.1, Except for Test 2 and L = 6

TABLE 4.3

LONGITUDINAL POSITION OF ε'_{max} FROM t_o TO $t_o + 36$ FOR ALL TEST RUNS

	t_o	t_o+12	t_o+24	t_o+36
Case A				
L = 3	28.1	22.5	42.2	16.9
L = 6	30.9	28.1	25.3	22.5
Case B				
L = 3	28.1	42.2	11.3	25.3
L = 6	36.6	5.6	19.7	33.8
Test 1				
L = 3	5.6	5.6	2.8	0.0
L = 6	8.4	8.4	5.6	5.6
Test 2				
L = 3	5.6	42.2	5.6	16.9
L = 6	28.1	45.0	8.4	2.8
Test 3				
L = 3	8.4	8.4	11.3	16.9
L = 6	8.4	8.4	2.8	0.0
Test 4				
L = 3	5.6	42.2	5.6	14.1
L = 6	2.8	0.0	8.4	2.8
Test 5				
L = 3	8.4	8.4	8.4	2.8
L = 6	2.8	5.6	8.4	8.4
Test 6				
L = 3	2.8	5.6	8.4	33.8
L = 6	2.8	8.4	0.0	45.0

upper level maximum except at t_o + 36 where the lower maximum is lagging behind the upper maximum. However, this seems to be an anomaly. Overall, the movement and vertical structure of the perturbed vorticity maxima appear to move with the mean wind speed in both cases.

2. Nonlinear Tests

Tests 3 and 4 evaluated the nonlinear mountain experiments. All initial conditions are similar to tests 1 and 2 except for the added wavenumbers 0 and 16. Figures 4.9 and 4.10 compare the nonlinear perturbed vorticity for both nonlinear cases as well as the linear cases at both levels. Inspection of these figures as well as Table 4.1 shows that the nonlinear wind reversal case, test 3 has considerably less growth than the linear case at both sigma levels. A vertical comparison reveals that the lower sigma level, L = 6, shows stronger growth rates in the linear and nonlinear modes for the wind reversal situation versus the upper level. Thus both modes show strong low-level cyclonic development in the first 30 h. This is not the situation for the non-wind reversal cases, tests 2 and 4. The growth rates are relatively small at both atmospheric levels. Overall the linear case, test 1, experiences the largest growth at L = 6, the lower level.

Further inspection of Figures 4.9 and 4.10 reveals that the nonlinear cases, tests 3 and 4 experienced considerable dampening after t_o + 30 (approx. 66 h), while

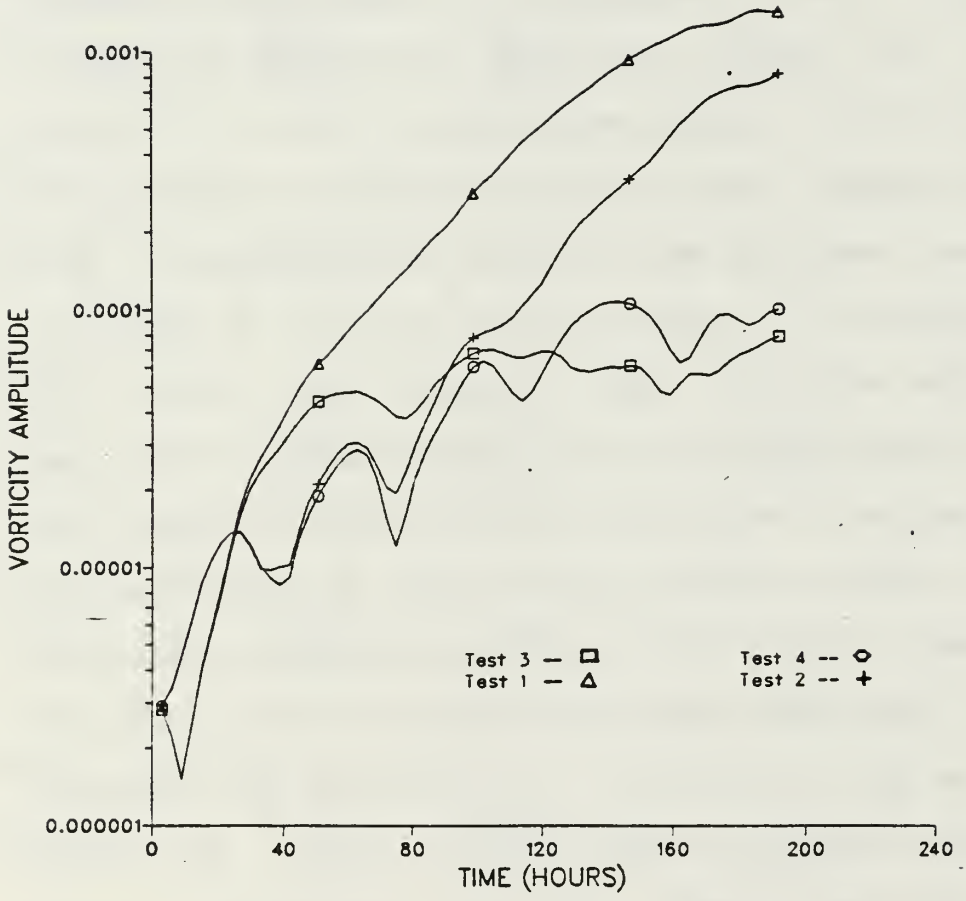

Figure 4.9 Same as Figure 4.1, Except for Tests 1, 2, 3 and 4 at L = 3

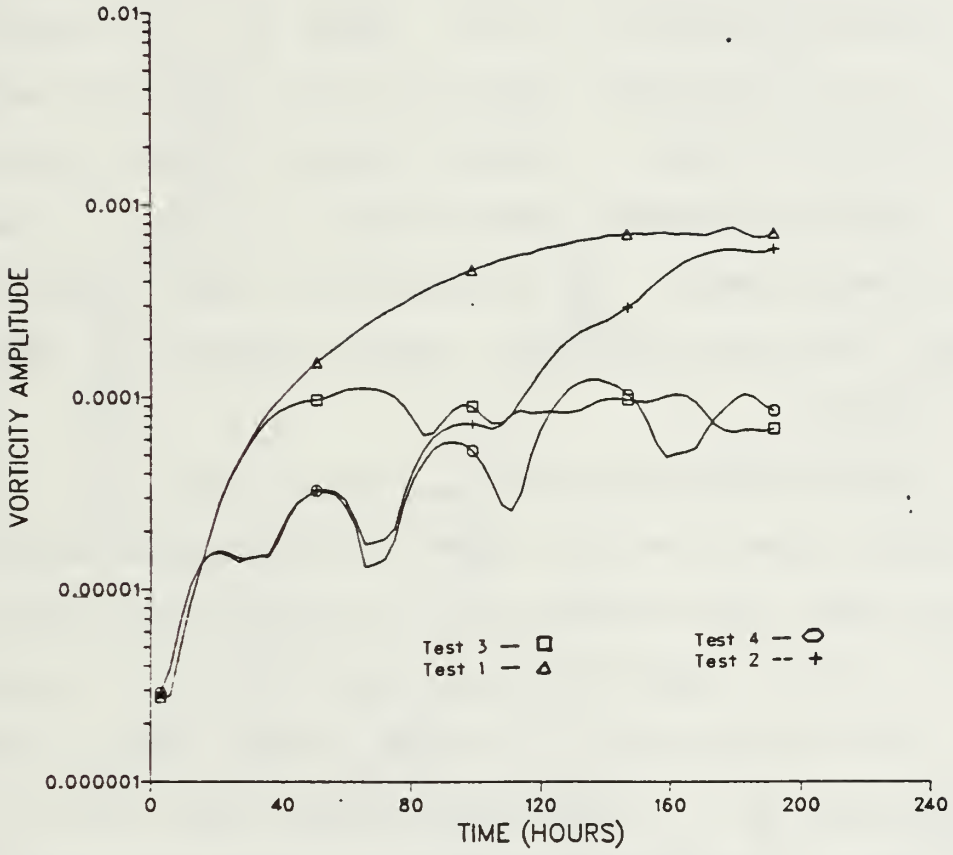

Figure 4.10 Same as Figure 4.1, Except for Tests 1, 2, 3 and 4 at L = 6

the linear cases increased exponentially throughout. Another feature observed is the undulation pattern in all the non wind-reversal cases. This may be due to the forced mountain solution imposed on the pure baroclinic solution.

Examination of the phase speed (Figures 4.11, 4.12, 4.13 and 4.14) reveals that test 3 at L = 3 exhibits stationary movement from t_o to t_o + 9, followed by a positive movement through t_o + 80. After t_o + 80 there appears to be an oscillation about the 25° longitude but this is difficult to verify. However, test 3 at the lower level has a similar negative phase speed to test 1, the linear wind reversal case. The non-reversal cases, tests 2 and 4, show comparable positive phase speeds at both tropospheric levels.

The vertical structure of ξ'_{max} shows that test 3, the wind reversal case, has the upper level maximum ahead (east) of the lower level maximum due to the positive phase speed at L = 3 and a negative phase speed at L = 6 (see Table 4.3). This decoupling is unique in this study and cannot be explained here. In the non-reversal case, test 4, there is at least a consistent stacking of the two levels where the upper level trails the lower level maximum at t; however, due to a slightly faster phase speed at L = 3, the upper-level maximum moves ahead of the lower-level maximum by t_o + 30.

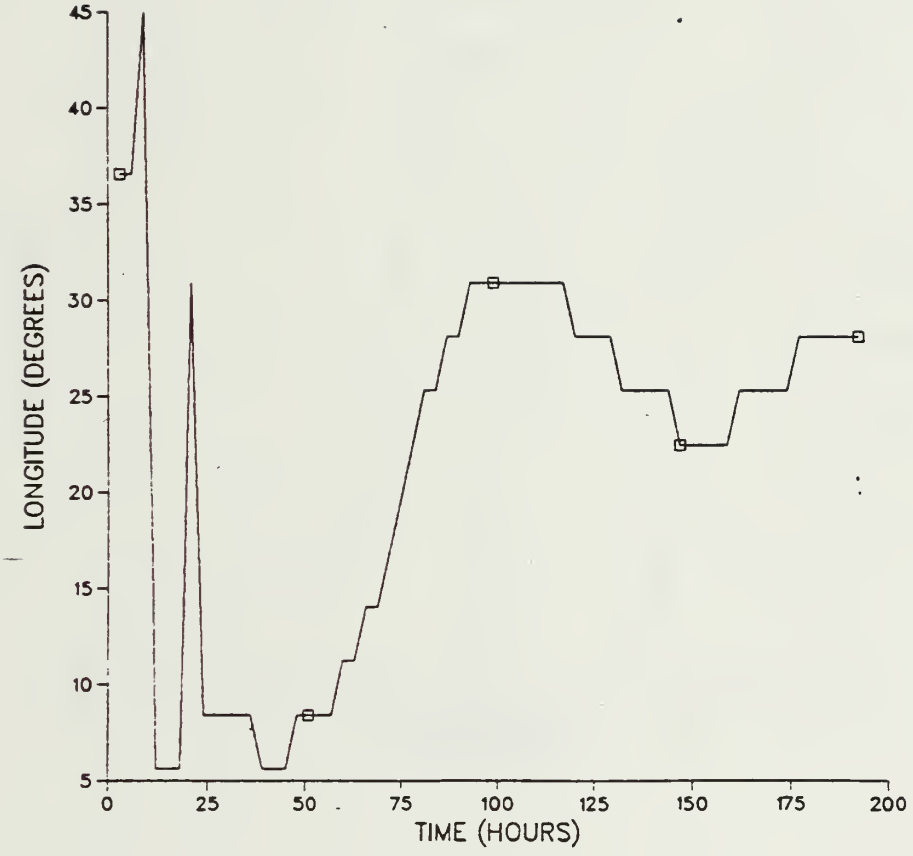

Figure 4.11 Test 3; Longitudinal Phase Position of ξ'_{max} vs. Time at L = 3

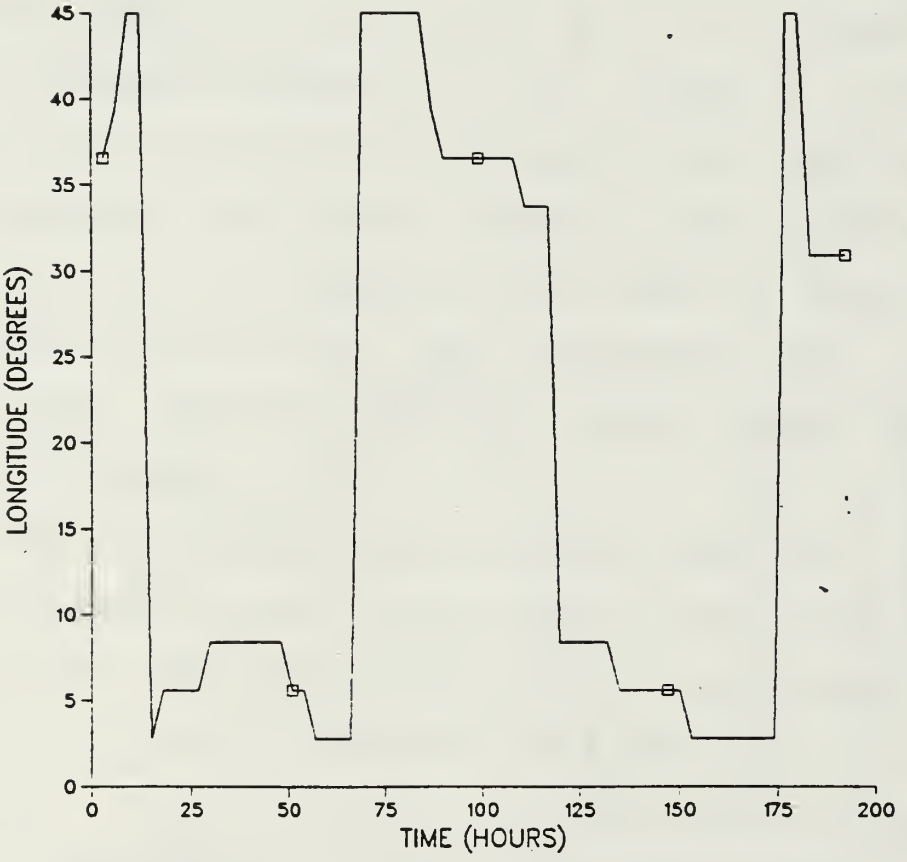

Figure 4.12 Same as Figure 4.11, Except for L = 6

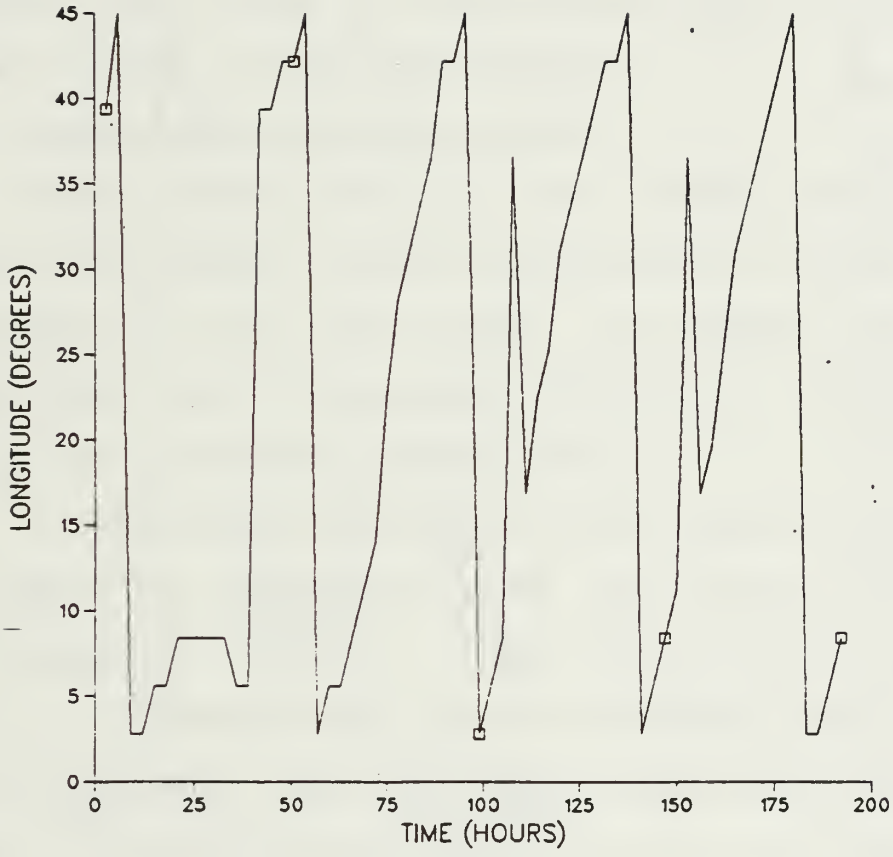

Figure 4.13 Same as Figure 4.11, Except for L = 3

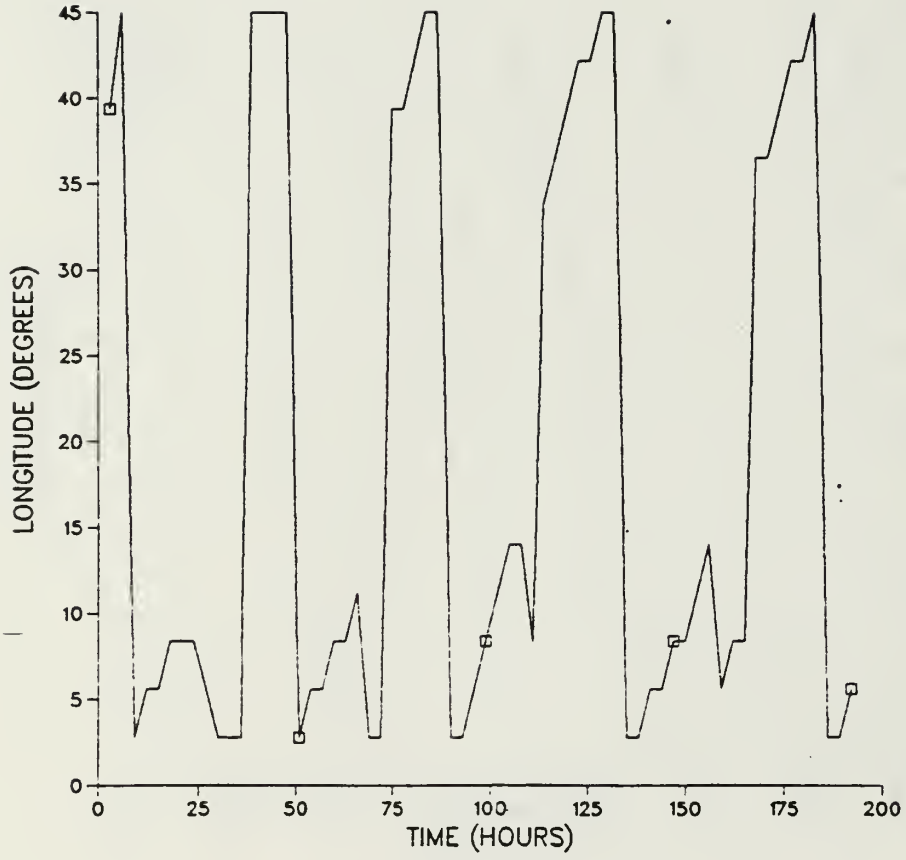

Figure 4.14 Same as Figure 4.11, Except for L = 6

Overall comparison reveals that through the first 36 h both wind reversal cases, tests 1 and 3 agree qualitatively except for the curious meandering phase speed at the upper level in test 3 (the nonlinear wind reversal experiment). Another significant finding is that the growth is more than twice as large for the wind reversal studies at the lower level versus the upper level, while the opposite is found for the non-reversal studies.

3. Rapid Mountain Growth Tests

These studies have the same initial conditions of the previous studies except the mountain is raised to its full height in just three hours. The purpose is to help identify the large fluctuations induced by inertial gravity waves in the linearized spectral model.

Inspection of the results from Figures 4.15 and 4.16 shows rapid and relatively large oscillations of ξ'_{max} at both atmospheric levels. These oscillations appear to dampen to a relatively low value by the 15th hour at L = 3 and by the 8th hour at L = 6. ξ'_{max} exhibits the most growth in test 5, the wind reversal case, at the lower level. This appears consistent with the previous wind reversal mountain experiments. In the non-reversal studies the short mountain growth period does not affect the qualitative results which shows that test 6 agrees quite closely with tests 2 and 4 where the upper-level growth is greater than at the lower level.

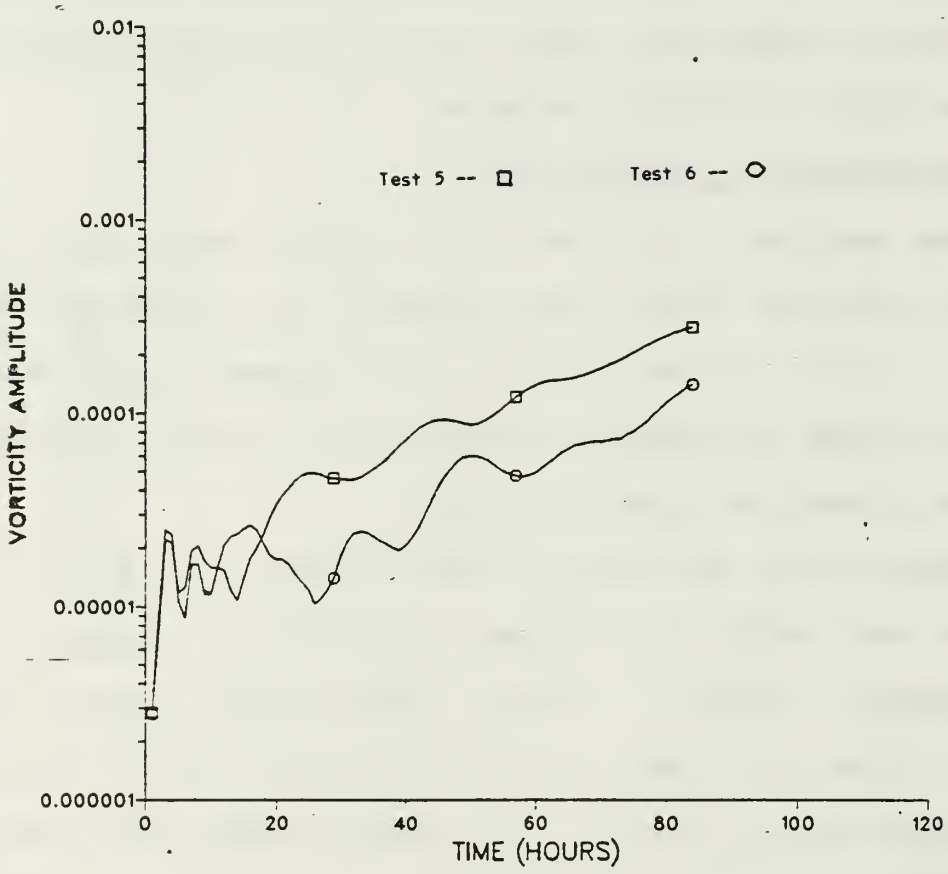

Figure 4.15 Same as Figure 4.1, Except for Tests 5 and 6 at L = 3

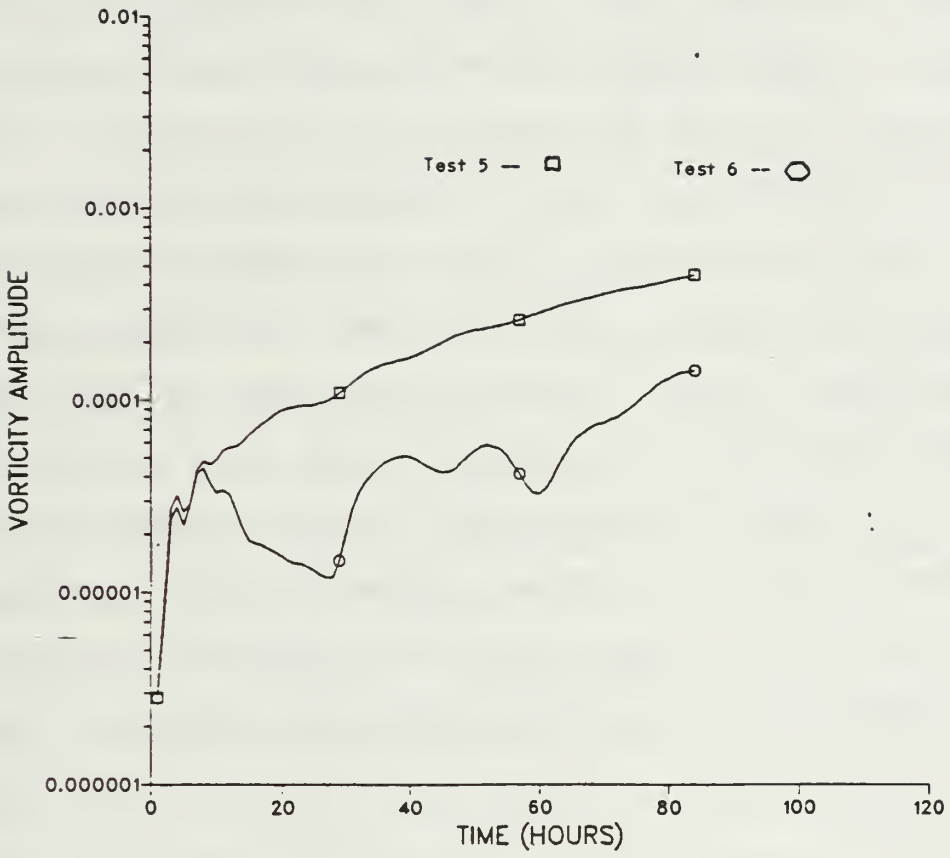

Figure 4.16 Same as Figure 4.1, Except for Tests 5 and 6 at L = 6

The phase speeds for both wind profiles are also compatible with the previous studies. The only deviation observed is in test 5 which retrogresses considerably more at the lower level (L = 6).

A vertical analysis (Table 4.3) shows consistent vertical stacking from t_o (3rd hour) to t_o + 36 (39th hour) for the wind reversal test. The non-reversal case also shows a similar stack through the same period, and it begins to move rapidly away from the mountain in unison by t_o + 39.

From inspection of all six mountain experiments the most significant results ar that the wind reversal profiles can be twice as conducive to low-level vorticity growth versus upper-level growth, and the phase speeds of the wind reversal investigations also appear to be more favorable, since they are closer to stationarity (in particular test 5) which would allow the time necessary for cyclone intensification (i.e., there would be sufficient time for the growing vortex to interact with the basic flow).

V. CONCLUSIONS

The objective of this research is to determine whether a wind profile which reverses direction in the vertical can lead to stronger leeside cyclogenesis, than a profile which does not reverse. One basis of this study is the work by Smith (1986) who determined that a wind backing with height (i.e., a vertical wind profile through a cold front) is more conducive to cyclone growth. Smith (1986) utilized a quasi-geostrophic linear model. He imposed a lid which simulated the tropopause to allow for baroclinic instability. He found that a lid at 10 km with a wind reversal profile produced the most significant cyclonic growth. This study used a primitive equation baroclinic spectral model in both linear and nonlinear modes. This was done to see the computational difference of the two modes as well as to compare the linear results with other studies, such as Smith (1986). The nonlinear mode also allows an evaluation of the impact of wave interactions that appear in the real atmosphere.

Two control tests were performed how a wind reversal and non wind-reversal profile behaved with no topography. Six mountain experiments were then tested: The first two (reversal and non-reversal) were in the linear mode (wavenumber 8) with the mountain allowed to grow to its full

height in 36 h. The next two tested were run with the same parameters as the first set, except the model was in the nonlinear mode (wavenumbers 0, 8, 16). The last two tests were run in the linear mode but the mountain grew to its full height in just three hours. The last set was used to find out whether the inertial gravity waves in this primitive equation model would seriously affect the growth of a leeside vortex in contrast to the first four mountain tests.

It was found that the most rapid growth of a leeside cyclone, as measured by the maximum deviation from the longitudinally averaged vorticity (ξ'_{max}), occurred in the linear wind reversal case (Test 1). The nonlinear wind reversal case (Test 3) grew just as rapidly in the first 12 hours but, as expected, the nonlinear wave interactions dampened growth thereafter. For the non-reversal cases (Tests 2 and 4), ξ'_{max} did not grow as quickly. In addition, it was observed that the growth at the lower atmospheric level (L = 6) was normally twice that at the higher atmospheric level (L = 3) for all wind reversal cases.

This study also investigated the movement (phase speed) of ξ'_{max}). One major finding is that nearly all wind reversal experiments (tests 1, 3 and 5) had a relatively slow retrograding ξ'_{max}, in particular the short mountain growth experiment (Test 5) at the lower atmospheric level. In contrast, the movement of ξ'_{max} for all the non-reversal

cases was positive and quite fast, i.e., ξ'_{max} was moving away from the favored position for leeside development quite rapidly during the first 30 h. Thus the wind reversal tests had more favorable phase speeds during the preferred time of leeside cyclogenesis. The only test which did not seem to behave in the same manner as the others was Test 3, the nonlinear wind reversal case, which showed a large positive phase speed at the upper level (L = 3) and thus it appeared that the two atmospheric levels were decoupled. All other tests exhibited a coupling between the lower and upper atmospheric perturbed vorticity maximums since the phase speeds at both levels were quite similar.

Based on the results of this study, it appears there is good support for favorable leeside development when a wind reversing with height is present. However, more studies need to be carried out. The factors to be explored might include: (1) masking the orographic forced solution to isolate the pure perturbation field by itself; (2) a more realistic scenario involving a more accurate terrain model of the Alps; and (3) a jet structure consistent with the observed conditions when leeside development occurs in that region, e.g., southwesterly flow aloft and northwesterly flow at the surface rather than the artificial wind structure in this study.

This study dealt with a jet structure with specific vertical wind profiles and a mountain ridge (2213 m high)

perpendicular to the initial mean flow. It examined the growth of leeside cyclones based on the maximum deviation from the longitudinal averaged vorticity. A more reasonable indicator of growth might be the maximum deviation from the time averaged vorticity. Although the mountain appeared high enough and long enough to include the effects of low level blocking, a higher ridge greater than 3000 m might be more realistic. The effects of a latent heat source which might represent the Gulf of Genoa could be included in a future model to see its effect on cyclone intensification. All these factors could possibly affect the growth of a leeside low.

LIST OF REFERENCES

Arakawa, A., and M. Suarez, 1983: Vertical differencing of the primitive equations in sigma coordinates. Mon. Wea. Rev., 111, 34-45.

Eady, E., 1949: Long waves and cyclone waves. Tellus, 3, 33-52.

Haltiner, G.J., and R.T. Williams, 1980: Numerical Prediction and Dynamical Meteorology. John Wiley and Sons, Inc., New York, 477 pp.

Hayes, J.L., 1985: A Numerical and Analytical Investigation of Lee Cyclogenesis. Ph.D. Thesis, Department of Meteorology, Naval Postgraduate School, Monterey, California, 138 pp.

Lubeck, O., T. Rosmond, and R.T. Williams, 1977: Divergent initialization experiments using a spectral model. Naval Postgraduate School Technical Report NPS-63Wu7791, 81 pp.

Smith, R.B., 1984: A theory of lee cyclogenesis. J. Atmos. Sci., 41, 1159-1168.

Smith, R.B., 1986: Further development of a theory of lee cyclogenesis. J. Atmos. Sci., 43, 1582-1602.

Walker, J.P., 1982: Numerical Simulation of the Influence of Small Scale Mountain Ranges on a Baroclinic Wave. Master's Thesis, Naval Postgraduate School, Monterey, California, 159 pp.

INITIAL DISTRIBUTION LIST

		No. Copies
1.	Defense Technical Information Center Cameron Station Alexandria, Virginia 22304-6145	2
2.	Library, Code 0142 Naval Postgraduate School Monterey, California 93943-5002	2
3.	Meteorology Reference Center (Code 63) Department of Meteorology Naval Postgraduate School Monterey, California 93943-5000	1
4.	Chairman (Code 63Rd) Department of Meteorology Naval Postgraduate School Monterey, California 93943-5004	1
5.	Dr. Roger T. Williams, Code 63Wu Department of Meteorology Naval Postgraduate School Monterey, California 93943-5004	3
6.	USAF ETAC/LD Air Weather Service Technical Library Scott AFB, Illinois 62225-5000	1
7.	Program Manager (AFIT/CIR) Air Force Institute of Technology Wright-Patterson AFB, Ohio 45433	1
8.	Commander Air Weather Service Scott AFB, Illinois 62225	1
9.	Commander Air Force Global Weather Central Offutt AFB, Nebraska 68113	1
10.	Commander Naval Oceanography Command NSTL Station Bay St. Louis, Missouri 39522	1

11. Chief of Naval Research 1
    800 N. Quincy Street
    Arlington, Virginia 22217

12. Commanding Officer 1
    Naval Environmental Prediction
      Research Facility
    Monterey, California 93943-5000

13. Commanding Officer 1
    Fleet Numerical Oceanography Center
    Monterey, California 93943-5000

14. Commanding Officer 1
    Naval Ocean Research and
      Development Activity
    NSTL Station
    Bay St. Louis, Missouri 39522

15. Prof. Ronald B. Smith 1
    Yale University
    New Haven, Connecticut 06511

16. Professor M.A. Rennick, Code 63Rn 2
    Department of Meteorology
    Naval Postgraduate School
    Monterey, California 93943-5004

17. Capt. Gerald T. Byrne 2
    304 McKinley
    Norwood, Pennsylvania 19074

Thesis
B9565 Byrne
c.1 Numerical investigation of orographically enhanced instability.